Electrocatalysis (2024) 15:239–250
https://doi.org/10.1007/s12678-024-00870-1

RESEARCH

Evaluation of Pt–Rh Nanoparticle–Based Electrodes for the Electrochemical Reduction of Nitrogen to Ammonia

Roumayssa Amrine[1] · Miguel A. Montiel[1] · Vicente Montiel[1] · José Solla-Gullón[1]

Accepted: 28 March 2024 / Published online: 6 April 2024

Abstract

Ammonia (NH_3) is one of the most used chemicals. Industrially, ammonia is produced by hydrogenation of N_2 through the Haber–Bosch process, a process in which enormous amounts of CO_2 are released and requires a huge energy consumption (~2% of the total global energy). Therefore, it is of paramount importance to explore more sustainable and environmentally friendly routes to produce NH_3. The electrochemical nitrogen reduction reaction (NRR) to ammonia represents a promising alternative that is receiving great attention but still needs to be significantly improved to be economically competitive. In this work, the NRR is studied on Pt–Rh nanoparticle–based electrodes. Carbon-supported Pt–Rh nanoparticles (2–4 nm) with different Pt:Rh atomic compositions were synthesized and subsequently airbrushed onto carbon Toray paper to fabricate electrodes. The electrochemical NRR experiments were performed in a H-cell in 0.1 M Na_2SO_4 solution. The results obtained show interesting faradaic efficiencies (*FE*) towards NH_3 which range between 5 and 23% and reasonable and reliable NH_3 yield values of about 4.5 μg h^{-1} mg_{cat}^{-1}, depending on the atomic composition of the electrocatalysts and the metal loading. The electrodes also showed good stability and recyclability (constant *FE* and NH_3 yield in five consecutive experiments).

Keywords Electrocatalysis · Nitrogen reduction · Ammonia · Pt–Rh · Nanoparticles

Introduction

Ammonia (NH_3) is one of the world's most commonly produced industrial chemicals (150 million metric tons in 2019) [1] due to its important role as a fertilizer in the agricultural industry, the manufacture of pharmaceuticals, plastics, textiles, explosives and many other chemicals. NH_3 is also considered as a solution for the carbon-free chemical energy for the transportation sector [2–5]. Naturally, the production of ammonia from air and water at ambient temperature and pressure is limited only to some bacteria and plants through the nitrogen cycle [6, 7]. On the other hand, industrial NH_3 has been obtained through the Haber–Bosch process over the last 100 years, one of the most significant industrial chemical reactions that ever took place in the twentieth century, and which literally changed the world [8]. Nevertheless, reacting high purity streams of nitrogen (N_2) and hydrogen (H_2) not only requires extremely high temperatures (300–500 °C) and pressure (150–200 atm)—this process is responsible for approximately 2% of global energy consumption—but also produces significant amounts of greenhouse gases (mainly CO_2) [9]. Therefore, less energy demanding and more environmentally friendly strategies for the NH_3 production are needed [10, 11]. Among other alternatives, the electrochemical nitrogen reduction reaction (NRR) [12, 13] appears as an interesting option since it can be performed at low temperature and pressure without any CO_2 emissions and could be also powered with renewable energy sources [14–16]. However, the NRR is still a very challenging reaction due to multiple aspects including (i) high bonding energy of the N≡N triple bond (941 kJ mol^{-1}) [17], (ii) a weak solubility of the nitrogen (N_2) gas in water [18], (iii) NRR is multi-step process involving six electrons and six protons (in acidic electrolytes) with a sluggish kinetics [19],

$$N_2(g) + 6H^+(aq) + 6e \leftrightarrows 2NH_3(g)$$

and (iv) the competitive hydrogen evolution reaction (HER), a two-electron process, which is more kinetically preferred than the NRR [19],

✉ José Solla-Gullón
jose.solla@ua.es

[1] Institute of Electrochemistry, University of Alicante, Apdo. 99, 03080 Alicante, Spain

$2H^+(aq) + 2e \leftrightarrows H_2(g)$

among others. Consequently, the activity and selectivity of NRR are usually very low. However, relevant advances have been made in recent years and which have been reported in some recent reviews [20–26]. Among other aspects, the development of more active, selective, and stable to improve the faradaic efficiency (*FE*) and the ammonia yield rate r(NH_3) for NH_3 production is mandatory [21, 25–28]. It is well-established that noble metal electrocatalysts have been applied largely for diverse reactions considering their strong binding capacity for a great variety of reactants, adding to this their good electrical conductivity. Some examples of the application of noble metal electrocatalysts for NRR include ruthenium (Ru) [29], rhodium (Rh) [30], gold (Au) [31] and platinum (Pt) [32] electrocatalysts. Among these and based on density functional theory (DFT) calculations, Rh is well placed on top of the volcano plot of the ammonia synthesis, suggesting that metallic Rh would be a promising NRR catalyst due to its appropriate nitrogen-adsorption energy and low overpotential [33, 34]. In fact, Rh-based electrocatalysts have been recently evaluated for NRR [35–42]. In this sense, Liu et al. demonstrated that atomically thin Rh nanosheets are effective electrocatalysts for NRR with a high NH_3 yield rate of 23.9 μg h^{-1} $mg_{cat}{}^{-1}$ although the *FE* was only 0.2% [40]. Also, Su et al. demonstrated that the Rh-phosphide (Rh-P) catalyst achieved a high NH_3 yield of 37 μg h^{-1} $mg_{cat}{}^{-1}$ and a *FE* of about 7.6% [41]. Interestingly, Chung et al. reported the synthesis of a rhodium decorated molybdenum oxide (RhMoOx/C) electrocatalyst for an efficient NRR with high selectivity. RhMoOx/C catalyst exhibited an outstanding NH_3 yield rate of 57.2 μg h^{-1} $mg_{cat}{}^{-1}$ at − 0.6 V vs RHE and a high *FE* of about 22% [42]. On the other hand, it is also known that Pt-based electrocatalysts are not the most convenient electrocatalysts for NRR [33]. This is because Pt is currently considered one of the best materials for the competitive HER [43, 44]. This explains the almost absence of works using Pt electrocatalysts for NRR [25, 26, 32]. However, some works have recently shown that Pt can exhibit enhanced NRR activity when subjected to modification with another substance [45, 46]. For this reason, in this work, we explored the use of Pt–Rh nanoparticles with different atomic percentages for the NRR. In addition, the preference for utilizing these metals and alloys in the nanoparticulated form is grounded in the vast literature on the use of nanoparticulate systems in electrocatalysis. It is well known that nanomaterials have a special structure that exposes a lot of active sites compared to traditional bulk catalysts making them advantageous for various catalytic reactions such as the NRR. Adding to this is the design flexibility of low-dimensional nanocatalysts, as their surface structures and electronic properties exhibit high sensitivity to particle size and morphology [47, 48]. In this way, carbon-supported Pt, Rh and Pt–Rh (with different atomic compositions) nanoparticles (Pt–Rh/C NPs) were successfully synthesized and physicochemical and electrochemically characterized. Subsequently, Pt–Rh nanoparticle–based electrodes were manufactured and used to study the electrochemical reduction of nitrogen to ammonia in 0.1 M Na_2SO_4 as the electrolyte solution. *FE* and NH_3 yields were systematically evaluated. It is worth noting that several blank experiments were conducted to warrant the results obtained and avoid NH_3 contamination. NH_3 contamination is one of the main problems in NRR and has been the subject of very relevant contributions [49–53]. Finally, some stability tests were also carried out with the most convenient Pt:Rh electrode.

Experimental

Chemicals and Reagents

For the nanoparticles synthesis, rhodium(III) chloride hydrate (Sigma-Aldrich) and chloroplatinic acid hydrate ($H_2PtCl_6{\cdot}6H_2O$; Thermo Scientific Chemicals) were used as Rh and Pt precursors respectively. N-heptane (Fisher Chemical), Brij L4 (Sigma-Aldrich) and sodium borohydride ($NaBH_4$ 99%, Aldrich) were used as solvent, surfactant and reducing agent respectively. Vulcan XC-72 carbon powder (CAS No 1333–86-4, sample number GP 3621) was purchased from Cabot Corporation (Boston, MA, USA) and used as support material for the metallic nanoparticles. Na_2SO_4 (99.5%, Fisher Chemical) was used as supporting electrolyte in the catholyte and anolyte solutions, while sulfuric acid (95–97% Emsure ISO) was used for the NH_3 acid trap solution. A cationic ion exchange membrane Nafion 112 (DuPont, Wilmington, DE, USA) was activated in 0.5 M KOH (86.5% VWR chemicals) and used as a separator in the H-cell electrochemical cell (CS932S, Corrtest Instrument). All chemicals were used as received without any further purification. All solutions were prepared using Milli-Q ultrapure water (18.2 MΩ cm).

Synthesis of Pt/Rh Nanoparticles

The methodology used for the synthesis of the Pt/Rh nanoparticles is similar to that previously used in our research group with other metals and takes place at room temperature and pressure [54]. The nanoparticles were obtained by reduction of the corresponding metal precursors with sodium borohydride ($NaBH_4$) using a n-heptane/BrijL4/water microemulsion. In a first step, the microemulsion was prepared from BrijL4, n-heptane and the precursor solution of the required metals under magnetic stirring. Subsequently, the reducing agent $NaBH_4$ was added in solid form. Once

the reducing agent was added, the solution was placed in an ultrasound bath for 15 min to complete the reduction process. After the addition of the reducing agent, the solution almost instantaneously becomes dark, indicating the reduction of Rh and Pt. Next, the necessary amount of carbon (Vulcan XC-72R) to obtain samples with a metal content of 30 wt% was added and stirred for at least 1 h under magnetic stirring and ultrasound. Finally, a volume of acetone that tripled that of the solution was added to achieve the separation of the phases. The precipitate formed by the metallic nanoparticles was subjected to a chemical decontamination treatment to clean them. The samples were washed and rinsed with acetone, acetone:water mixtures (50:50) and finally ultrapure water [54]. In this way, a good removal of the residual surfactant molecules present in the nanoparticles is achieved. The nanoparticles were left to dry in the oven at 65 °C for 24 h. The yield obtained was calculated before preparing the catalytic inks. The reactive amounts for the synthesis of 150 mL of the different metal nanoparticles are reported in the supporting information (Table S1).

Preparation of Pt, Rh and Pt–Rh Electrodes

For the manufacture of the electrodes, a catalytic ink was prepared containing the Pt/C, Rh/C and Pt–Rh/C NPs, Nafion solution (perfluorosulfonic acid — PTFE copolymer 5% w/w solution, Alfa Aesar) as binder with a NPs/C:Nafion mass ratio of 80:20 and diluted to 2 wt% in absolute ethanol (EMSURE®, Merck, Darmstadt, Germany). The mixture was sonicated for 30 min, and the ink was directly sprayed by airbrushing technique onto a Toray paper (TGPH-90 from QuinTech, Göppingen, Germany) with a geometric surface area of 6.25 cm^2 (2.5 cm × 2.5 cm). The airbrushing spraying is carried out in a hot metallic plate at 90 °C to facilitate solvent evaporation. The final NPs/C loadings were 1.2 mg cm^{-2}, 0.8 mg cm^{-2} and 0.4 mg cm^{-2}.

Physicochemical Characterization

Dispersion, morphology and size of the nanoparticles were studied with transmission electron microscopy (TEM) with a JEOL JEM-1400 Plus microscope (JEOL, Akishima, Tokyo, Japan) working at 120 kV. X-ray photoelectron spectroscopy (XPS) experiments were recorded on a K-Alpha spectrometer (Thermo Scientific, Waltham, MA, USA) using AlKα 1486.6 eV radiation, monochromatized by a twin crystal monochromator and yielding a focused X-ray spot with a diameter of 400 mm, at 3 mA × 12 kV. Deconvolution of the XPS spectra was carried out using a Shirley background. The different metal Pt, Rh and Pt–Rh loadings were experimentally analysed by inductively coupled plasma optical emission spectrometry (ICP-OES) (PerkinElmer, Optima 4300 D). For that, a known amount of the carbon supported Pt, Rh and Pt–Rh nanoparticles was firstly treated in aqua regia and then in 35% hydrochloric acid to dissolve the Pt and Rh. The corresponding solutions were then diluted using a 2-wt% HCl water solution and finally filtered before being analysed. Scanning electron microscopy (JEOL microscope, IT500HR/LA with EDS detector) was employed to analyse the morphology of the electrocatalytic layer of the manufactured electrodes. X-ray diffraction (XRD) patterns were obtained with a Bruker D8 Advance diffractometer fitted with a copper tube. The optical setup included a Ni 0.5% CuKβ filter in the secondary beam so that only CuKα radiation illuminated the sample ($CuK\alpha_1 = 0.154059$ nm and $CuK\alpha_2 = 0.154445$ nm). The sample was measured in reflection geometry over the 20–90° 2θ range with a step of 0.10° and a counting time of 15 s per step.

Electrochemical Characterization

The electrochemical characterization of the Pt, Rh and Pt–Rh-based electrodes was performed in a three-electrode configuration glass cell in Ar-saturated 0.5 M H_2SO_4 (95–97% Emsure ISO) solution and in Ar and N_2-saturated 0.1 M Na_2SO_4 (99.5%, Fisher Chemical) solution using a platinum wire and a leakless AgCl/Ag (Saturated KCl) as counter and reference electrodes respectively. Cyclic voltammetry (CV) experiments were performed using a PGSTAT302N system (Metrohm Autolab B. V., Utrecht, the Netherlands). All CV measurements were performed at room conditions. Portions of about 3 cm^2 of the different electrodes were used during the electrochemical measurements. The current density was normalized to this geometric area.

Electrochemical Synthesis of Ammonia

N_2 electroreduction was performed in an H-type electrochemical cell with divided compartments through a cationic ion exchange membrane (Nafion 112). A N_2-saturated 0.1 M Na_2SO_4 was used as catholyte and anolyte. A 1-mM H_2SO_4 solution was used to collect the NH_3 that is present in the cathodic gas phase thus preventing the loss of any produced NH_3. The Nafion 112 membrane was previously activated in 0.5 M KOH for 24 h. A platinum wire immersed in the anolyte acted as counter electrode. A leakless AgCl/Ag (saturated KCl) electrode placed in the catholyte was used as reference electrode. Portions of about 3 cm^2 of the different electrodes were used in the nitrogen electrolyses. The nitrogen gas (N_2) utilized in the experiments possesses a high purity grade of 99.999%. The current density was normalized to this geometric area. The N_2 electroreduction electrolyses were carried out by setting at controlled potential between − 0.04 and − 0.34 V vs RHE for 2 h using a PGSTAT302N system (Metrohm

Autolab B. V., Utrecht, the Netherlands). Moreover, two bubblers containing 0.1 M $KMnO_4$ and 0.1 M KOH were connected in series at the entrance of the cell to capture and prevent any NOx contaminations and false positives of NH_3 coming from the nitrogen gas cylinder [40–44]. Fig. S1 shows the experimental setup employed for the NRR. It is also worth noting that all glassware was initially cleaned with a saturated $KMnO_4$ solution, to strip organic species, metals and other N_2 species from the glassware. Then, the glassware is rinsed with a diluted H_2O_2/H_2SO_4 solution and finally boiled two–three times in ultrapure water.

Analytical Determination and Estimation of Faradaic Efficiency and Ammonia Yield

The quantification of ammonia produced both in the electrochemical cell and in the acidic trap is performed by the "Indophenol blue" method using a HACH Lange DR-3800 system [55]. After the electrolyses, 5 mL from the cathodic chamber and the acidic collector was pipetted out and added to the commercial analysis tubes (LCK 304 Ammonium), where ammonium ions react at pH 12.6 with hypochlorite ions and salicylate ions in the presence of sodium nitroprusside as a catalyst to form indophenol blue. The analysis tubes were kept in the dark for 15 min before UV–Vis spectrophotometric measurements. Standard $(NH_4)_2SO_4$ solutions was used to calibrate the concentration-absorbance curve (Fig. S2). As indicated by the supplier, the detection limit of this "Indophenol blue" method using a HACH Lange DR-3800 system, and the commercial analysis tube (LCK 304 Ammonium) is 0.015 mg/L NH_4-N. The calculation of faradaic efficiency (*FE*) and ammonia yield rate ($r(NH_3)$) was carried out using the following equations:

Faradaic efficiency (*FE*)

$$FE = \frac{3F \times m(\mathrm{NH_3})}{17 \times Q} \times 100\%$$

Ammonia yield rate ($r(NH_3)$)

$$r(\mathrm{NH_3}) = \frac{[\mathrm{NH_{4^+}}] \times V}{t \times m(\mathrm{cat})}$$

where F is the Faraday constant (96,485 C mol^{-1}); $m(NH_3)$ is the concentration of ammonia in the electrolyte (mol); Q is the amount of electricity consumed in the electrolysis process (C); $[NH_4^+]$ is the concentration of ammonia in the electrolyte (μg mL^{-1}); V is the volume of the electrolyte (mL); t is the electrolysis time (h); and m(cat) is the mass of electrocatalyst (PT + Rh) on the electrode (mg).

Control Experiments to Determine Nitrate, Nitrite and Ammonia Contamination

To ensure that ammonia comes from the electrochemical nitrogen experiments and not from impurities, several blank and control experiments were systematically and routinely performed at every key step of the experiments. In detail, (i) control experiments were performed by bubbling only N_2 gas through the electrochemical cell in the absence of electrodes and, obviously, potential control. This control experiment is of outstanding importance to guarantee the absence of NOx and ammonia contaminations in the flow of N_2 that enters the electrochemical system from the N_2 gas cylinder. At this respect, high-performance liquid chromatography measurements were performed to quantify the presence of nitrite (NO_2^-) and nitrate (NO_3^-). These analyses were carried out using a HPLC 1100 Series with an anion column Metrosep A Supp 4 — 250/2.0 with a UV detector at 225 nm and a 1.7-mM Na_2CO_3/1.8-mM $NaHCO_3$ aqueous solution mobile phase at 1 ml/min. These HPLC measurements indicate that the Milli-Q ultrapure water used in this work is free of detectable amounts of NO_2^- and NO_3^- impurities (Fig. S3). However, it is worth noting that the 0.1 M Na_2SO_4 solution used as catholyte showed a NO_3^- contamination of about 0.65 ppm, whereas NO_2^- remained undetectable (Fig. S4). Nitrate and nitrite calibration plots are shown in Fig.S5. Interestingly, our control experiments by bubbling only N_2 gas for 2 h through the electrochemical cell in the absence of electrodes indicate that bubbling N_2 does not increase the amount of NO_2^- and NO_3^- in the electrolyte and that the amount NH_3 remained undetectable (Table S1). Also, (ii) to find out whether the NH_3 obtained with the Pt–Rh electrodes effectively comes from the N_2 electroreduction or from the NO_3^- impurities detected in our electrolyte, new control experiments were performed in which Ar gas is bubbled through the electrolyte into the electrochemical cell for 2 h under electrochemical operation using a $Pt_{70}Rh_{30}$/C electrode and applying a potential of − 0.12 V vs RHE. The results are reported in Table S2 and evidence that, despite the presence of NO_3^- impurities, NH_3 still remains undetectable indicating that our electrochemical system does not convert NO_3^- into NH_3. Also, as shown in Table S2, the NO_3^- concentration remained unaltered at about 0.65 ppm. If any amount of ammonia is detected after these control experiment, the system is considered and "contaminated". In this case, a thorough cleaning of all materials is undertaken, followed by the repetition of the control experiments. These control experiments enable the identification of potential sources of contamination such as the glassery, the membrane and the electrodes prior their use. Also, it is worth mentioning that the ammonia generated in the cathodic compartment can easily cross the cationic membrane, facilitated by the cation exchange mechanism, and migrate to the anodic

chamber [56]. To check this point, an analysis of the anolyte is routinely conducted and, if quantities of NH_3 are identified, the membrane undergoes a washing procedure, and the experiment is subsequently repeated. It is worth mentioning that these blank/control experiments are systematically run both before the beginning of a new series of experiments and during the intervals between successive experiments with positive results. In this way, a positive result is always placed between two blank experiments with negative results (in terms of ammonia detection). The work protocol used in this contribution is schematically summarized in Fig. S6.

Results and Discussion

Characterization of the Pt–Rh/C Nanoparticles

The synthesis of Pt, Rh and Pt–Rh nanoparticles is detailed in the "Experimental" section and Table S3. Seven samples were prepared: Pt/C, $Pt_{80}Rh_{20}$/C, $Pt_{70}Rh_{30}$/C, $Pt_{50}Rh_{50}$/C, $Pt_{30}Rh_{70}$/C, $Pt_{20}Rh_{80}$/C and Rh/C. The particle size, morphology and dispersion of the different nanoparticles were studied with transmission electron microscopy (TEM). Figure 1 shows some representative TEM images of the samples. In all cases, the nanoparticles display a quasi-spherical morphology and are reasonably well dispersed on the carbon support although some agglomeration is also observed. To estimate the mean diameter of the nanoparticles, about 100–150 particles from different TEM images were analysed. The corresponding particle size histograms are reported in Fig. S7. The mean particle size of the different nanoparticles is depicted in Fig. 1 and ranges from 3 to 5 nm.

On the other hand, to study the surface chemistry of our material, X-ray photoelectron spectroscopy (XPS) measurements were also performed to obtain information on the oxidation state of Pt and Rh in the bimetallic mixture as well as the atomic ratio of both metals (Fig. S8; Table 1). From the response due to the analyses of Pt 4f spectra, and for all the bimetallic samples, it is observed that two main contributions can be observed. For the Pt $4f_{7/2}$ spectral line, the main peak at a binding energy of 71.5 ± 0.2 eV is attributable to Pt(0) species and the other peak at 72.7 ± 0.2 eV attributable to Pt(II) species. The results indicate that Pt is mainly in its metallic state and that the relative concentration of this PtO is around 15–20%. The presence of Rh induces a small, but clear shift of about 0.3–0.1 eV to higher binding energies of the Pt 4f XPS peaks, thus suggesting a certain modification of the electronic environment of Pt with the incorporation of Rh on the nanoparticles. For Rh 3d, the Rh $3d_{5/2}$ spectral line shows the presence of two peaks with binding energies located at 307.4 ± 0.1 and 308.4 ± 0.2 eV. These binding energies can be attributed to Rh(0) and Rh(III) respectively. In this case, very small differences are observed in terms of BE as a function of Pt concentration, suggesting that there is not a significant modification of the electronic properties of Rh with the change of the composition of the nanoparticles.

XPS experiments were also employed to determine the atomic composition of Pt:Rh nanoparticles. Table 1 shows the results obtained. These results clearly indicate that the real atomic composition of the samples is in good agreement with the expected nominal atomic composition calculated from the mixture of the Pt and Rh precursors. Since the XPS results mainly correspond to the superficial composition of the nanoparticles, ICP-OES measurements were also performed to calculate the bulk composition of the different Pt:Rh nanoparticles (Table 1). As can be seen in Table 1, XPS and ICP-OES results are very similar. These findings confirm that no surface enrichment of any element (Pt or Rh) is observed in the prepared nanoparticles. Also, the ICP-OES analyses allow the actual metal loading of the samples to be determine. These results are reported in Table S4. For the monometallic samples, the actual metal loading was similar to the nominal one (about 30 wt%). However, for the bimetallic samples, the actual metal loading was clearly lower which could be attributed to a loss of sample during the extensive washing steps.

X-ray powder diffraction (XRD) patterns of the different Pt/Rh nanoparticles are shown in Fig. S9. For the two pure metal Pt and Rh nanoparticles, their diffraction peaks can be indexed with their corresponding face-centred cubic structure except for the broad peak at about 26–27° 2θ which is due to the carbon power. The results obtained with the Pt–Rh nanoparticles shows a clear evolution of the position of their diffraction lines between the limiting values corresponding to the two pure metals (Pt and Rh).

Characterization of the Nanoparticle-Based Electrodes

The different Pt/C, Rh/C and Pt–Rh/C nanoparticles were used to manufacture the corresponding nanoparticle-based electrodes by air-brushing technique using a Toray carbon paper (TGPH-90) as carbon substrate. The experimental details are described in the experimental section. Electrodes with a loading of 1.2 $mg_{catalyst}\ cm^{-2}$ were initially prepared. The surface of the electrodes was characterized by scanning electron microscopy (SEM) to evaluate how the catalytic inks cover the Toray paper substrates. The SEM analyses also include an energy dispersive X-ray (EDX) Pt and/or Rh mapping of the XY plane section of the electrodes. The different SEM/EDX images are shown in Fig. S10. The results obtained indicate that the catalytic ink covers the carbon fibres homogeneously, showing a uniform and compact catalytic layer with some slight agglomerations in the case of $Pt_{80}Rh_{20}$/C and $Pt_{50}Rh_{50}$/C, probably due to imperfections in the air-brush process. EDX mappings also display

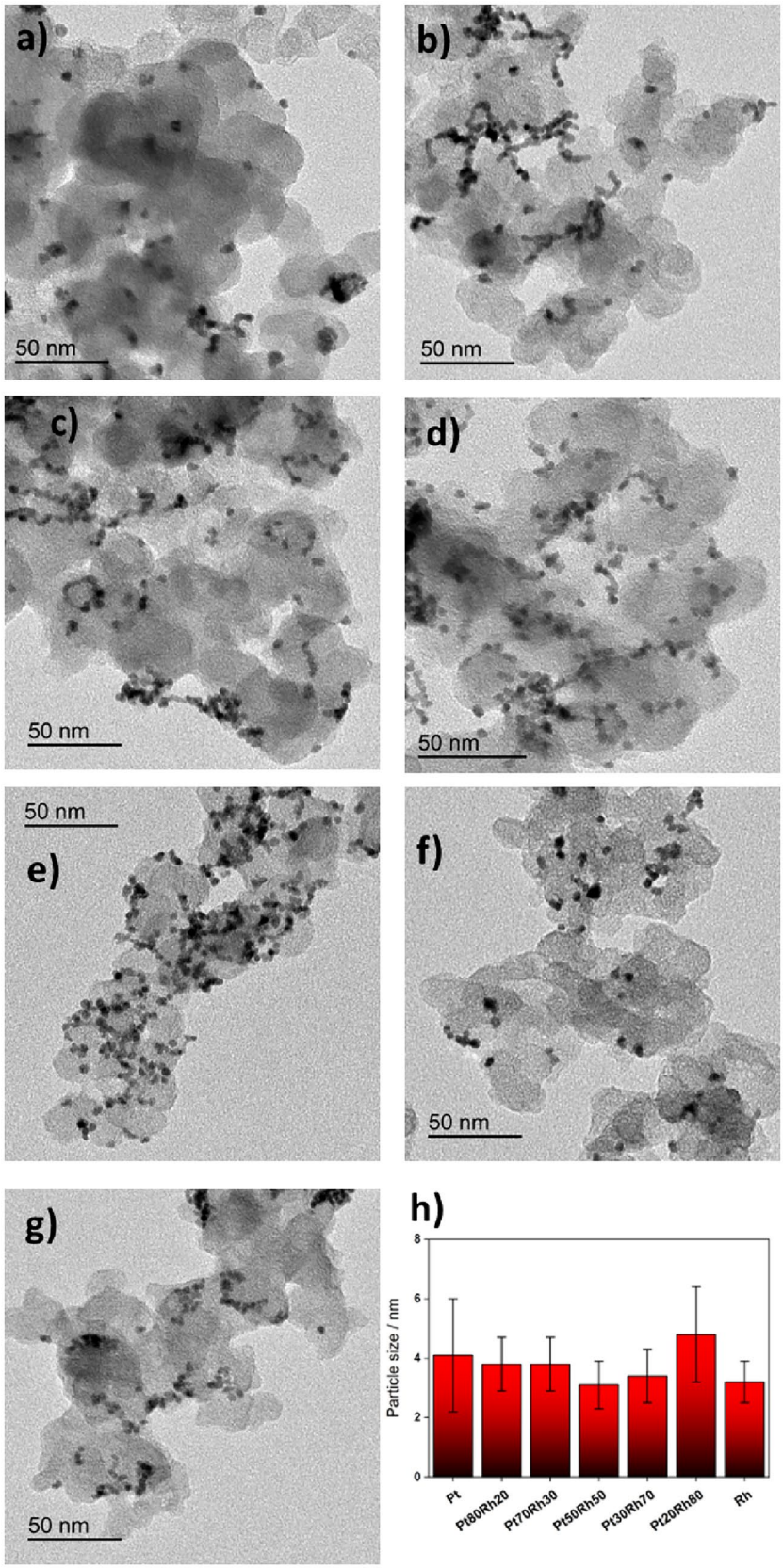

Fig. 1 Representative TEM images of **a** Pt/C, **b** $Pt_{80}Rh_{20}$/C, **c** $Pt_{70}Rh_{30}$/C, **d** $Pt_{50}Rh_{50}$/C, **e** $Pt_{30}Rh_{70}$/C, **f** $Pt_{20}Rh_{80}$/C, and **g** Rh/C nanoparticles, and **h** mean particle size of the different Pt–Rh nanoparticles

Table 1 Quantitative XPS and ICP-OES data for Pt/Rh nanoparticles

Nominal atomic composition	Atomic composition from XPS	Atomic composition from ICP-OES
Pt_{100}/C	Pt_{100}/C	Pt_{100}/C
$Pt_{80}Rh_{20}$/C	$Pt_{85}Rh_{15}$/C	$Pt_{86}Rh_{14}$/C
$Pt_{70}Rh_{30}$/C	$Pt_{70}Rh_{30}$/C	$Pt_{71}Rh_{29}$/C
$Pt_{50}Rh_{50}$/C	$Pt_{57}Rh_{43}$/C	$Pt_{52}Rh_{48}$/C
$Pt_{30}Rh_{70}$/C	$Pt_{35}Rh_{65}$/C	$Pt_{38}Rh_{62}$/C
$Pt_{20}Rh_{80}$/C	$Pt_{24}Rh_{76}$/C	$Pt_{28}Rh_{72}$/C
Rh_{100}/C	Rh_{100}/C	Rh_{100}/C

a homogeneous distribution of Pt and Rh depending on the corresponding atomic composition of the sample.

Electrochemical Characterization of the Electrodes

Before performing the N_2 reduction electrochemical experiments, it is very important to verify the cleanness of the electrodes as well as to assess the voltammetric responses of the different electrodes. This can be conveniently evaluated by recording the voltammetric response of the different electrodes in 0.5 M H_2SO_4. Fig. S11 shows the voltammetric profiles of the electrodes before (black line) and after (red line) being washed with an additional cleaning step with 1 M NaOH. The alkaline cleaning treatment has been shown to be very effective for the removal of many different capping agents [56–59]. It is worth mentioning that these electrochemical experiments were performed without iR compensation, and therefore, the voltammograms look slightly resistive. The results indicate that whereas for some electrodes such as $Pt_{50}Rh_{50}$ and $Pt_{20}Rh_{80}$, their electroactive surface areas clearly increase after the alkaline treatment; for the others, the additional cleaning is less important and the voltammetric response before and after the NaOH cleaning are very similar. This evidences that, although the nanoparticles were subjected to the same decontamination treatment (see the "Experimental" section), some samples are cleaner than others. The additional alkaline cleaning guaranties the good cleanness of the samples before being used for the nitrogen electrochemical reduction experiments. From the point of view of the voltammetric profiles, the electrodes display a clear evolution from the characteristic features associated with a polyoriented Pt surface to those associated with a polyoriented Rh one. These results are in good agreement with previous findings [56, 60, 61] and are correlated with the gradual modification of the surface atomic composition of the Pt:Rh nanoparticles (Table 1). It is also worth noting that for the Pt-rich electrodes, the HER is accompanied by the hydrogen oxidation reaction (HOR) when the potential scan shifts towards positive values (at potential around

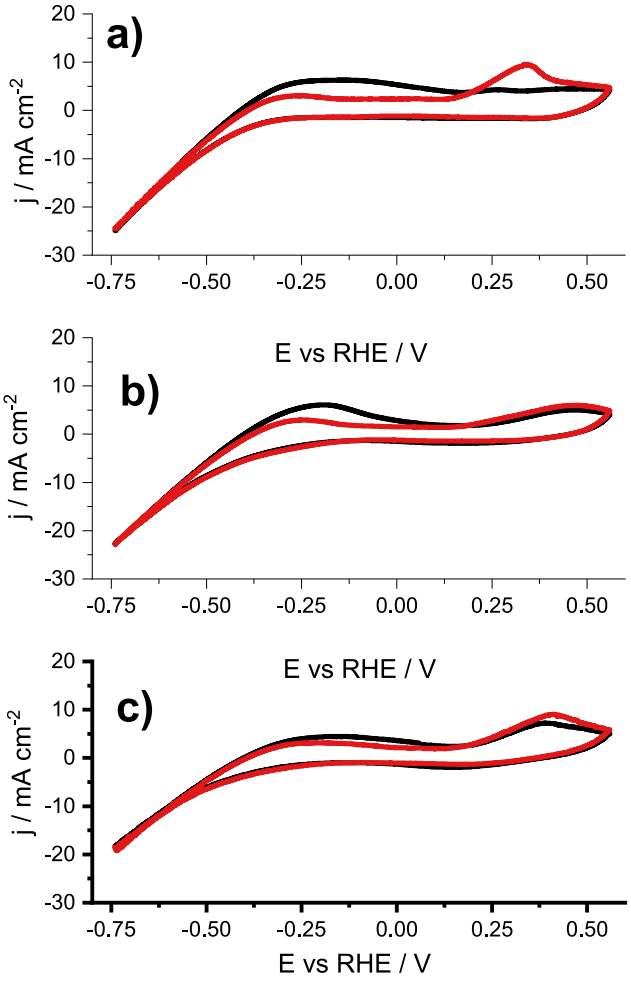

Fig. 2 Cyclic voltammograms obtained in Ar (black line) and N_2 (red line) saturated 0.1 M Na_2SO_4 solution with **a** Pt/C-, **b** $Pt_{50}Rh_{50}$/C-, and **c** Rh/C-based electrodes. Scan rate 50 mV s^{-1}

0.0 V vs RHE). This HER/HOR region is less visible for the Rh-rich electrodes. Subsequently, the electrochemical response of the different electrodes in Ar (black line) and N_2 (red line) saturated 0.1 M Na_2SO_4 solution was obtained. Figure 2 shows the voltammetric profiles corresponding to Pt, $Pt_{50}Rh_{50}$ and Rh. The complete collection of voltammograms is shown in Fig. S12. These voltammograms were recorded between − 0.74 and 0.56 V vs RHE. This potential range allows clearly visualizing the HER on the samples in the negative potential region. In the positive potential region, the upper potential is limited to 0.56 V vs RHE to avoid the surface oxidation of the nanoparticles. In the potential range of interest for NRR (from 0 V to − 0.25 V which corresponds to the onset potential for the HER), the voltammetric responses of the electrodes in Ar (black line) and N_2 (red line) saturated 0.1 M Na_2SO_4 solution are very similar, without any distinctive feature related to nitrogen reduction, and only with a slightly increase of the negative currents in the N_2 saturated solution. However, in the positive scan, the oxidation currents are always (independently of the composition of the electrode) higher in Ar than in N_2. The origin

of this finding is not clear and still requires more studies. To better study the NRR to ammonia on the different electrodes, N_2 reduction electrolyses experiments were performed at different potentials of interest.

Chronoamperometric Measurements

N_2 electroreduction electrolysis experiments were conducted in a H-type electrochemical cell in N_2 saturated solution at − 0.04, − 0.12, − 0.14, − 0.24 and − 0.34 V vs RHE for 2 h. The experimental details are included in the experimental section. Before each electrolysis, five voltammetric cycles between 0.56 and − 0.74 V vs RHE were recorded at 50 mV s^{-1} to verify the status of the electrodes. Four of the potentials studied are placed in the potential range of interest for NRR (from 0 V to − 0.25 V which corresponds to the onset potential for the HER). Also, an additional potential (− 0.34 V vs RHE) has been also studied for which the HER is more predominant. At less negative potential values than − 0.34 V, the *FE* for ammonia production is negligible. The chronoamperometric results are reported in Fig. S13. As expected, for all electrodes, currents in the potential range between 0 and − 0.25 V are relatively low and rather stable in comparison with currents obtained at − 0.34 V for which HER dominates the electrochemical response and where some decay in current is observed. The *FE* and NH_3 yield values obtained in all these measurements are reported in Fig. S14. In addition, for the sake of comparison, Fig. 3 compares some of the most relevant findings extracted from Fig. S14. It is worth recalling that a 1-mM H_2SO_4 solution is used as ammonia trap connected to the gas exhaust of the cell and that the amount of NH_3 both produced in the cell and collected in the ammonia trap is measured by the indophenol blue method [55].

Regarding the *FE*, the results clearly confirm that, as previously mentioned, at − 0.34 V vs RHE, the process is HER dominated and, consequently, the *FE* are close to zero for all electrodes. For the other potentials, the *FE* towards ammonia ranges from 2 to 10% depending on the nature of the electrode. Comparing the pure Pt/C and Rh/C samples, it is observed that unexpectedly Pt (maximum *FE* about 7%) behaves slightly better than Rh (maximum *FE* about 4%). In both cases, FEs decay for increasing negative potentials. For the Pt:Rh electrodes, it is observed that whereas the $Pt_{80}Rh_{20}$/C displays a behaviour similar to Pt/C, in terms of *FE* values and *FE* evolution with the potential, the other electrodes show some different properties and the *FE* presents a maximum value between − 0.04 and − 0.14 V vs RHE and then decay. The highest *FE* values obtained for the different samples are reported in Fig. 3. Among them, the $Pt_{70}Rh_{30}$/C displays a maximum *FE* value of about 10–11%. Also, it is worth noting that, except for the $Pt_{50}Rh_{50}$/C, the behaviour of the Pt:Rh electrodes is better than the behaviour of the pure elements. This means that a synergetic effect is taking place which could be tentatively explained by the role of Pt in

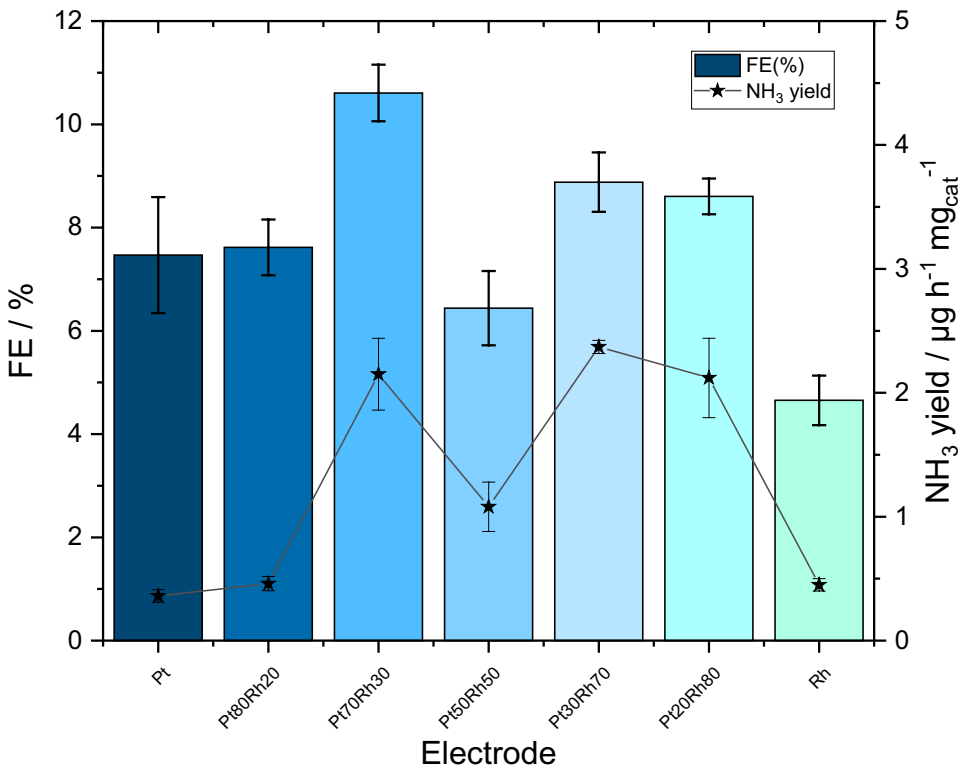

Fig. 3 Comparison of the FEs and NH_3 yield values for the different electrocatalysts with a loading of 1.2 mg cm^{-2}

promoting the adsorption of hydrogen molecules on the surface of the nanoparticles; Pt is currently considered one of the best electroactive materials for HER [39] and, on the other hand, because Rh has good energetic properties for the NRR as previously reported in the volcano plots available in the literature [21, 26, 33, 34]. The combination of both effects, which ought to be necessary to the formation of ammonia, may lead to the proposed synergetic effect and explain the results obtained.

In terms of NH_3 yield, the values obtained were very low for all electrodes and ranged from 0.5 to 3–4 μg h^{-1} mg_{cat}^{-1} in the best cases. Again, the results obtained with the Pt:Rh electrodes are better than the results obtained with the pure elements which were found to be systematically less than 1 μg h^{-1} mg_{cat}^{-1} independently of the applied potential. Unexpectedly, all these NH_3 yield values were rather low in comparison to some previous findings [25, 26, 40–42]. For instance, for atomically thin Rh nanosheets, a good NH_3 yield rate of 23.9 μg h^{-1} mg_{cat}^{-1} was obtained [40]. A similar value of about 20.4 μg h^{-1} mg_{cat}^{-1} was reported for a nanoporous Pd hydride electrocatalyst at − 0.15 V vs. RHE in 0.1 M phosphate buffer solution [62]. Also, for Bi nanospheres, a value of 23.4 μg h^{-1} mg_{cat}^{-1} was found at − 0.4 V vs. RHE in 0.1 M Na_2SO_4 [63]. These low NH_3 performance results made us think that something was not working correctly in our electrodes. Among other possible aspects, the effect of the electrode loading was explored. In this sense, it is noteworthy that while numerous studies have investigated the impact of different factors on electrolysis experiments such as pH, temperature, electrolyte, stirring and gas flow, there has been limited discussion on the influence of electrode loading on the intrinsic activity obtained experimentally. Considering that the electrodes were prepared by airbrushing technique onto a Toray paper, that is, by accumulation of layers, a high loading could give rise to important mass transport problems of the reactants to the inner parts of the electrodes and, consequently, to a low N_2 reduction performance. This phenomenon was recently studied by Yu et al. for the oxygen evolution reaction (OER) with Co_3O_4 electrocatalysts loaded on a glassy carbon electrode (GCE) [64]. By using different loadings, they demonstrated that for increasing loadings, the apparent OER activity decreased as consequence of the (a) increase of the distance for the transport of electrons over the electrode, (b) decrease of the accessibility of the electrocatalyst towards the electrolyte and (c) ion diffusion limitations. In this way, to check this hypothesis, two new $Pt_{70}Rh_{30}$/C electrodes of different loadings (0.8 and 0.4 mg cm^{-2}) were prepared, tested and compared with the results obtained with the same electrode with a 1.2-mg cm^{-2} loading under the same NRR working conditions ($E = -0.12$ V vs RHE, electrolysis time = 2 h). The results obtained are shown in Fig. 4.

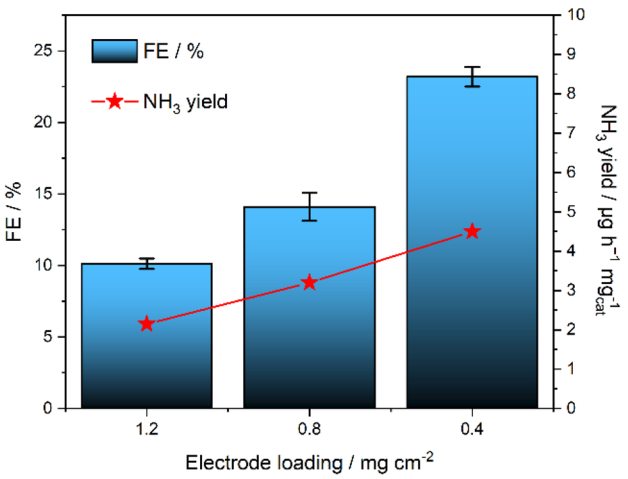

Fig. 4 Effect of the electrode loading on NH_3 production (*FE* and NH_3 yield) for the $Pt_{70}Rh_{30}$/C-based electrodes at − 0.12 V vs RHE in N_2 saturated 0.1 M Na_2SO_4 solution. Electrolysis time, 2 h

For these experiments, control experiments were also performed with a bare Toray paper electrode and a Toray paper with a layer of pure carbon (Vulcan XC-72R, loading about 0.8 mg cm^{-2}) to verify the no formation of NH_3. The results are shown in Figs. S15 (voltammetric profiles) and S16 (chronoamperometric measurements). The results indicate the absence of detectable ammonia during these control experiments. The results obtained (Fig. 4) clearly indicate that both *FE* and NH_3 yield remarkably increase for decreasing metal loadings. Thus, the *FE* increase from 10 to 23% when the loading decreases from 1.2 to 0.4 mg cm^{-2}. Likewise, the NH_3 yield continuously grows from 2.2 to 4.5 μg h^{-1} mg_{cat}^{-1} as loading decreases. In this way, in terms of *FE*, these values (about 23%) reveal some improvement in comparison to previous studies using Pt and Rh based electrodes for the NRR. For instance, Pt/NiO-2 samples exhibited a maximum *FE* of about 16% at − 0.2 V vs RHE [65], while a designed Rh atomic layer-decorated SnO_2 heterostructure electrocatalyst showed a *FE* of about 12% at − 0.3 V vs RHE [66]. However, in terms of NH_3 yield, even though the value has been doubled, the value obtained (4.5 μg h^{-1} mg_{cat}^{-1}) is still low in comparison to the values of 20.59 μg h^{-1} mg^{-1} and 149 μg h^{-1} mg_{cat}^{-1} reported for the Pt/NiO-2 samples [65] and Rh atomic layer–decorated SnO_2 heterostructures [66] respectively. Nevertheless, it is also important to note that similar and even lower NH_3 yield were also reported. For instance, Feng and coworkers found NH_3 yield values of about 4.5 μg h^{-1} mg^{-1} for and Pd/C and about 0.3 μg h^{-1} mg^{-1} for Au/C and Pt/C in 0.1 M neutral phosphate buffer solution (PBS) at − 0.05 V vs. RHE [67]. Also, for Ru-doped defect-rich SnO_2 nanoparticles deposited on carbon cloth, a value of 4.83 μg h^{-1} mg^{-1} was obtained at − 0.20 V vs. RHE in 0.1 M Na_2SO_4 [68]. In any case and taking into consideration recent

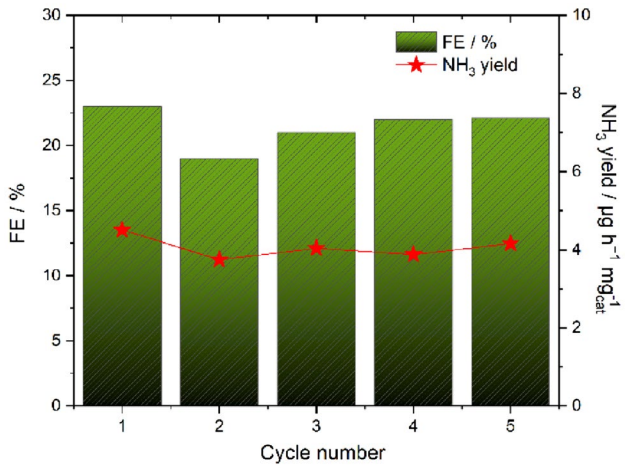

Fig. 5 Stability test of the $Pt_{70}Rh_{30}$/C-based electrode for five cycles of electrolysis (at − 0.12 V vs RHE during 2 h for every cycle) in N_2 saturated 0.1 M Na_2SO_4 solution

reviews [25, 26], the NH_3 yield values obtained here are low but reliable. This last question is of outstanding importance because, as stated in the introduction section, rigorous control experiments are required to minimize or even avoid the NH_3 contamination sources.

Stability of the Electrodes

Stability of the electrodes for NRR is a very important parameter that has been scarcely evaluated [20–26, 69, 70] and, therefore, still requires much more work. To evaluate the stability of electrode ($Pt_{70}Rh_{30}$/C electrode), the same portion of electrode has been tested for five consecutive chronoamperometric experiments at − 0.12 V vs RHE for 2 h. The results are reported in Fig. 5 and indicate that the *FE* and NH_3 yield remain relatively constant with a *FE* value of 21.4 ± 1.5% and a NH_3 yield of 4.1 ± 0.3 μg h^{-1} mg_{cat}^{-1}. These findings suggest a good stability and recyclability.

Conclusion

In this study, the use of Pt:Rh-based electrodes for the NRR to ammonia in 0.1 M Na_2SO_4 was studied. Carbon-supported Pt, Rh and Pt:Rh (with different atomic compositions) nanoparticles (about 3–5 nm) were prepared using water-in-oil microemulsions. The different nanoparticles were physicochemically characterized (TEM, XPS, XRD and ICP-OES) and subsequently used to fabricate electrodes using the airbrushing technique onto a Toray paper. These Pt:Rh-based electrodes were then electrochemically characterized to verify their surface cleanness as well as the correct evolution of the voltammetric profiles (in 0.5 M H_2SO_4) depending on their atomic composition. The NRR experiments to ammonia showed some activity and selectivity to ammonia. Several control experiments were conducted to guaranty the reliability of the measurements and to avoid NH_3 contamination. These control experiments allow us to reasonably prevent false positives. For electrodes with a 1.2-mg cm^{-2} loading, the Pt:Rh electrodes displayed a better performance than that obtained with the pure elements. A maximum *FE* of about 10–11% is found with the $Pt_{70}Rh_{30}$/C electrode. However, for all electrodes, the NH_3 yield was unexpectedly low. Additional experiments at lower loading (0.4 and 0.8 mg cm^{-2}) allowed obtaining improved *FE* of about 23% and reasonable and reliable NH_3 yield values of about 4.5 μg h^{-1} mg_{cat}^{-1}. Also, in terms of stability (five consecutive chronoamperometric experiments at − 0.12 V vs RHE for 2 h), the electrode showed a remarkable stable performance for the production of NH_3 (21.4 ± 1.5% (*FE*) and 4.1 ± 0.3 μg h^{-1} mg_{cat}^{-1} (NH_3 yield)). More work is still in progress to particularly improve the NH_3 yield by using a gas diffusion electrode (GDE) configuration. The use of these GDEs is being considered very promising to achieve high ammonia productions and overcoming the low solubility of N_2 that strongly affects the electrochemical NRR performance [21].

Supplementary Information The online version contains supplementary material available at https://doi.org/10.1007/s12678-024-00870-1.

Acknowledgements R. A. acknowledges the Ministry of Higher Education and Scientific Research of the People's Democratic Republic of Algeria for the financial support to carry out her PhD study at the University of Alicante, Spain.

Author contributions R.A.: investigation, methodology, data curation, writing—original draft. M.A.M.: investigation, methodology, writing—original draft. V.M.: visualization, supervision, writing—review and editing. J.S-G.: visualization, supervision, writing—review and editing.

Funding Open Access funding provided thanks to the CRUE-CSIC agreement with Springer Nature.

Availability of Data and Material The datasets are available from the corresponding author on reasonable request.

Declarations

Ethical Approval Not applicable.

Competing interests The authors declare no competing interests.

References

1. U.S. Geological Survey, Mineral commodity summaries. U.S. Geological Survey, 200 p., (2020). https://doi.org/10.3133/mcs2020
2. V. Pattabathula, J. Richardson, Chem. Eng. Prog. **112**, 69 (2016)
3. N. Yahya, P. Puspitasari, K. Koziol, P. Guiseppe, Adv. Struct. Mater. (2011). https://doi.org/10.4028/www.scientific.net/JNanoR.16.119
4. A. Klerke, C.H. Christensen, J.K. Nørskov, T. Vegge, J. Mater. Chem. (2008). https://doi.org/10.1039/B720020J
5. A.E. Yüzbaşıoğlu, C. Avşar, A.O. Gezerman, Curr. Opin. Green Sustainable Chem. (2022). https://doi.org/10.1016/j.crgsc.2022.100307
6. V. Rosca, M. Duca, M.T. DeGroot, M.T.M. Koper, Chem. Rev. (2009). https://doi.org/10.1021/cr8003696
7. B.K. Burgess, D.J. Lowe, Chem. Rev. (1996). https://doi.org/10.1021/cr950055x
8. J.W. Erisman, M.A. Sutton, J. Galloway, Z. Klimont, W. Winiwarter, Nature Geosci. (2008). https://doi.org/10.1038/ngeo325
9. R.B. Jackson, J.G. Canadell, C. Le Quéré, R.M. Andrew, J.I. Korsbakken, G.P. Peters, N. Nakicenovic, Nat, Clim. Change (2016). https://doi.org/10.1088/1748-9326/aa9662
10. C. Li, T. Wang, J. Gong, Trans. Tianjin Univ. (2020). https://doi.org/10.1007/s12209-020-00243-x
11. J.G. Chen, R.M. Crooks, L.C. Seefeldt, K.L. Bren, B.R. Morris, M.Y. Darensbourg, P.L. Holland, B. Hoffman, M.J. Janik, A.K. Jones, M.G. Kanatzidis, P. King, K.M. Lancaster, S.V. Lymar, P. Pfromm, W.F. Schneider, R.R. Schrock, Science (2018). https://doi.org/10.1126/science.aar6611
12. S. Giddey, S.P.S. Badwal, A. Kulkarni, Int. J. Hydrog. Energy (2013). https://doi.org/10.1016/j.ijhydene.2013.09.054
13. X. Cui, C. Tang, Q. Zhang, Adv. Energy Mater. (2018). https://doi.org/10.1002/aenm.201800369
14. J.N. Renner, L.F. Greenlee, A.M. Herring, K.E. Ayers, Electrochem. Soc. (2015). https://doi.org/10.1149/2.F04152if
15. D. Bao, Q. Zhang, F.L. Meng, H.X. Zhong, M.M. Shi, Y. Zhang, J.M. Yan, Q. Jiang, X.B. Zhang, Adv. Mater. (2017). https://doi.org/10.1002/adma.201604799
16. S. Ghavam, M. Vahdati, I.A.G. Wilson, P. Styring, Front. Energy Res. (2021). https://doi.org/10.3389/fenrg.2021.580808
17. X. Tang, Y. Hou, C.Y. Ng, B. Ruscic, J. Chem. Phys. (2005). https://doi.org/10.1063/1.1995699
18. R. Battino, T.R. Rettich, T. Tominaga, J. Phys. Chem. (1984). https://doi.org/10.1063/1.555713
19. X. Zhu, S. Mou, Q. Peng, Q. Liu, Y. Luo, C. Chen, S. Gao, X. Sun, J. Mater. Chem (2020). https://doi.org/10.1039/C9TA13044F
20. B.H.R. Suryanto, H.L. Du, D. Wang, J. Chen, A.N. Simonov, D.R. MacFarlane, Nat. Catal. (2019). https://doi.org/10.1038/s41929-019-0252-4
21. T. Wu, W. Fan, Y. Zhang, F. Zhang, Mater. Today Phys. (2021). https://doi.org/10.1016/j.mtphys.2020.100310
22. Y. Yang, W. Zhang, X. Tan, K. Jiang, S. Zhai, Z. Li, Coord. Chem. Rev. (2023). https://doi.org/10.1016/j.ccr.2023.215196
23. X. Yang, S. Mukherjee, T. O'Carroll, Y. Hou, M. R. Singh, J. A. Gauthier, G. Wu. Angew. Chem. Int. Ed. (2023) X. Yang, S. Mukherjee, T. O'Carroll, Y. Hou, M. R. Singh, J. A. Gauthier, G. Wu. Angew. Chem. Int. Ed. (2023) https://doi.org/10.1002/anie.202215938
24. S. Zhang, X. Zhang, C. Liu, L. Pan, C. Shi, X. Zhang, Z.F. Huang, J., J. Zou. Mater. Chem. Front. (2023). https://doi.org/10.1039/D2QM01061E
25. M.A. Mushtaq, M. Arif, G. Yasin, M. Tabish, A. Kumar, S. Ibraheem, W. Ye, S. Ajmal, J. Zhao, P. Li, J. Liu, A. Saad, X. Fang, X. Cai, S. Ji, D. Yan, Renew. Sustain. Energy Rev. (2023). https://doi.org/10.1016/j.rser.2023.113197
26. Z. Huang, M. Rafiq, A.R. Woldu, Q.X. Tong, D. Astruc, L. Hu, Coord. Chem. Rev. (2023). https://doi.org/10.1016/j.ccr.2022.214981
27. D. Liu, M. Chen, X. Du, H. Ai, K.H. Lo, S. Wang, S. Chen, G. Xing, X. Wang, H. Pan, Adv. Funct. Mater. (2021). https://doi.org/10.1002/adfm.202008983
28. C. Guo, J. Ran, A. Vasileff, S.Z. Qiao, Energy Environ. Sci. (2018). https://doi.org/10.1039/C7EE02220D
29. H. Tao, C. Choi, L.X. Ding, Z. Jiang, Z. Han, M. Jia, Q. Fan, Y. Gao, H. Wang, A.W. Roberston, S. Hong, Y. Jung, S. Liu, Z. Sun, Chem. (2019). https://doi.org/10.1016/j.chempr.2018.10.007
30. P. Shen, X. Li, Y. Luo, N. Zhang, X. Zhao, K. Chu, Appl. Catal. B (2022). https://doi.org/10.1016/j.apcatb.2022.121651
31. H. Wang, D. Yang, S. Liu, S. Yin, H. Yu, Y. Xu, X. Li, Z. Wang, L. Wang, ACS Sustainable Chem. Eng. (2019). https://doi.org/10.1021/acssuschemeng.9b05542
32. Y.J. Mao, F. Liu, Y.H. Chen, X. Jiang, X.S. Zhao, T. Sheng, J.Y. Ye, H.G. Liao, L. Wei, S.G. Sun, J. Mater. Chem. A (2021). https://doi.org/10.1039/D1TA05515A
33. E. Skúlason, T. Bligaard, S. Gudmundsdóttir, F. Studt, J. Rossmeisl, F. Abild-Pedersen, T. Vegge, H. Jónssonm, J.K. Nørskov, Phys. Chem. Chem. Phys. (2012). https://doi.org/10.1039/C1CP22271F
34. A.J. Medford, A. Vojvodic, J.S. Hummelshøj, J. Voss, F. Abild-Pedersen, F. Studt, T. Bligaard, A. Nilsson, J.K. Nørskov, J. Catal. (2015). https://doi.org/10.1016/j.jcat.2014.12.033
35. Y. Yao, S. Zhu, H. Wang, H. Li, M. Shao, Angew. Chem. Int. Ed. (2020). https://doi.org/10.1002/anie.202003071
36. C. Yang, B. Huang, S. Bai, Y. Feng, Q. Shao, X. Huang, Adv. Mater. (2020). https://doi.org/10.1002/adma.202001267
37. N. Zhang, L. Li, J. Wang, Z. Hu, Q. Shao, X. Xiao, X. Huang, Angew. Chem. Int. Ed. (2020). https://doi.org/10.1093/nsr/nwaa088
38. H. Yu, Z. Wang, W. Tian, Z. Dai, Y. Xu, X. Li, L. Wang, H. Wang, Mater. Today. Energy (2021). https://doi.org/10.1016/j.mtener.2021.100681
39. M. Jin, X. Zhang, X. Zhang, H. Zhou, M. Han, Y. Zhang, G. Wang, H. Zhang, Nano Res. (2022). https://doi.org/10.1007/s12274-022-4585-y
40. H.M. Liu, S.H. Han, Y. Zhao, Y.Y. Zhu, X.L. Tian, J.H. Zeng, J.X. Jiang, B.Y. Xia, Y. Chen, J. Mater. Chem. A. (2018). https://doi.org/10.1039/c7ta10866d
41. J. Su, H. Zhao, W. Fu, W. Tian, X. Yang, H. Zhang, F. Ling, Y. Wang, Appl. Catal. B (2020). https://doi.org/10.1016/j.apcatb.2020.118589
42. S. Chung, D.H. Seo, M. Choi, X. Mao, A. Du, K. Ham, S. Giddey, J. Lee, H.K. Ju, J. Electroanal. Chem. (2021). https://doi.org/10.1016/j.jelechem.2021.115157
43. J.N. Hansen, H. Prats, K.K. Toudahl, N. Mørch Secher, K. Chan, J. Kibsgaard, I. Chorkendorff, ACS Energy Lett (2021). https://doi.org/10.1021/acsenergylett.1c00246
44. C. Li, J.B. Baek, ACS Omega (2020). https://doi.org/10.1021/acsomega.9b03550
45. Y. Deng, Z. Xiao, Z. Wang, J. Lai, X. Liu, D. Zhang, Y. Han, S. Li, W. Sun, L. Wang, Appl. Catal B (2021). https://doi.org/10.1016/j.apcatb.2021.120047
46. W. Xiong, M. Zhou, H. Li, Z. Ding, D. Zhang, Y. Lv, Chinese. J. Catal. (2022). https://doi.org/10.1016/S1872-2067(21)63877-9
47. H. Shen, C. Choi, J. Masa, X. Li, J. Qiu, Y. Jung, Z. Sun, Chem. (2021). https://doi.org/10.1016/j.chempr.2021.01.009

48. J. Wen, L. Zuo, H. Sun, X. Wu, T. Huang, Z. Liu, J. Wang, L. Liu, Y. Wu, X. Liu, T.V. Ree, Nanoscale Adv. (2021). https://doi.org/10.1039/D1NA00426C
49. S.Z. Andersen, V. Čolić, S. Yang, J.A. Schwalbe, A.C. Nielander, J.M. McEnaney, K. Enemark-Rasmussen, J.G. Baker, A.R. Singh, B.A. Rohr, M.J. Statt, S.J. Blair, S. Mezzavilla, J. Kibsgaard, P.C.K. Vesborg, M. Cargnello, S.F. Bent, T.F. Jaramillo, I.E.L. Stephens, J.K. Nørskov, I. Chorkendorff, Nature (2019). https://doi.org/10.1038/s41586-019-1260-x
50. J. Choi, B.H.R. Suryanto, D. Wang, H.L. Du, R.Y. Hodgetts, F.M. Ferrero Vallana, D.R. MacFarlane, A.N. Simonov, Nat. Commun (2020). https://doi.org/10.1038/s41467-020-19130-z
51. H. Liu, N. Guijarro, J. Luo, J. Energy Chem. (2021). https://doi.org/10.1016/j.jechem.2021.01.039
52. A.J. Martín, F.L.P. Veenstra, J. Lüthi, R. Verel, J. Pérez-Ramírez, Chem. Catalysis (2021). https://doi.org/10.1016/j.checat.2021.10.002
53. Y. Li, Z. Wang, H. Ji, L. Zhang, T. Qian, C. Yan, J. Lu, Chinese. J. Catal. (2023). https://doi.org/10.1016/S1872-2067(22)64148-2
54. F.J. Vidal-Iglesias, J. Solla-Gullón, V. Montiel, J.M. Feliu, A. Aldaz, J. Power. Sources (2007). https://doi.org/10.1016/j.jpowsour.2007.06.015
55. D. Li, X. Xu, Z. Li, T. Wang, C. Wang, Trends. Analyt. Chem. (2020). https://doi.org/10.1016/j.trac.2020.115890
56. M. Leonardi, G. Tranchida, R. Corso, R.G. Milazzo, S.A. Lombardo, S.M.S. Privitera, Membr. J. (2022). https://doi.org/10.3390/membranes12100969
57. F.J. Vidal-Iglesias, R.M. Arán-Ais, J. Solla-Gullón, E. Herrero, J.M. Feliu, ACS Catal. (2012). https://doi.org/10.1021/cs200681x
58. A. Zalineeva, S. Baranton, C. Coutanceau, Electrochem. Commun. (2013). https://doi.org/10.1016/j.elecom.2013.07.022
59. M.A. Montiel, F.J. Vidal-Iglesias, V. Montiel, J. Solla-Gullón, Curr. Opin. Electrochem. (2017). https://doi.org/10.1016/j.coelec.2016.12.007
60. P. Rodriguez, F.D. Tichelaar, M.T.M. Koper, A.I. Yanson, J. Am. Chem. Soc. (2011). https://doi.org/10.1021/ja208264e
61. V.F. de Carmargo, E.H. Fontes, J. Nandenha, R.F.B. de Souza, A.O. Neto, Res. Chem. Intermed. (2020). https://doi.org/10.1007/s11164-019-04050-5
62. W. Xu, G. Fan, J. Chen, J. Li, L. Zhang, S. Zhu, X. Su, F. Cheng, J. Chen, Angew. Chem. (2020). https://doi.org/10.1002/anie.201914335
63. J. Wang, Y. Ren, M. Chen, G. Cao, Z. Chen, P. Wang, J. Alloys Compd. (2020). https://doi.org/10.1016/j.jallcom.2020.154668
64. L. Yu, S. Sun, H. Li, Z.J. Xu, Fundam Res. (2021). https://doi.org/10.1016/j.fmre.2021.06.006
65. W. Xiong, M. Zhou, H. Li, Z. Ding, D. Zhang, Y. Lv, H. Li, Chinese. J. Catal. (2022). https://doi.org/10.1002/chem.202200779
66. Y. Liu, L. Huang, Y. Fang, X. Zhu, J. Nan, S. Dong, ACS Appl. Mater. Interfaces (2022). https://doi.org/10.1021/acsami.1c25240
67. J. Wang, L. Yu, L. Hu, G. Chen, H. Xin, X. Feng, Nat. Commun. (2018). https://doi.org/10.1038/s41467-018-04213-9
68. Y. Sun, Q. Wu, H. Li, S. Jiang, J. Wang, W. Zhang, X. Song, B. Jia, J. Qiu, T. Ma, Carbon (2022). https://doi.org/10.1016/j.carbon.2022.04.026
69. M. Zhao, C. Guo, L. Gao, X. Kuang, H. Yang, X. Ma, C. Liu, X. Liu, X. Sun, Q. Wei, Inorg. Chem. Front. (2021). https://doi.org/10.1039/D1QI00328C
70. H. Ying, T. Chen, C. Zhang, J. Bi, Z. Li, J. Hao, J. Colloid Interf. Sci. (2021). https://doi.org/10.1016/j.jcis.2021.05.185